Sixth International Symposium on Turbulence and Shear Flow Phenomena
Seoul, Korea, 22-24 June 2009

MIXING ENHANCEMENT OF TURBULENT COAXIAL JETS BY INFLOW PULSATION

Seong Jae Jang
Department of Mechanical Engineering,
KAIST
373-1 Guseong-dong, Yuseong-gu, Daejeon, 305-701, Korea
sj_jang@kaist.ac.kr

Hyung Jin Sung
Department of Mechanical Engineering,
KAIST
373-1 Guseong-dong, Yuseong-gu, Daejeon, 305-701, Korea
hjsung@kaist.ac.kr

ABSTRACT

The objective of the present study was to investigate the effects of inflow pulsation on the flow characteristics and the mixing properties of a turbulent confined coaxial jet flows. Large eddy simulations were performed at Re = 9000, based on the bulk velocity and outer radius of annular jet. The mean velocity ratio of central to annular jets was 0.6. The pulsation at the inflow jets was generated by varying the flow rate. First, the inflow pulsation was applied at frequencies in the range $0.1 < St < 0.9$ while other parameters are fixed. The pulsation frequency responses were scrutinized by examining the phase- or time-averaged turbulent statistics. The pulsation frequencies of $St = 0.180$ and 0.327 gave the greatest enhancement in mixing and reduction of the reattachment length, respectively. Then, the effects of the phase difference between two inflow jets at the two optimal frequencies were investigated. The inner and outer Kelvin-Helmholtz vortices were investigated in detail to observe the effects of the coherent structures on the mixing enhancement and the reduction of the reattachment length. The optimal conditions of the phase difference in the mixing enhancement and the reduction of the reattachment length were obtained when the strength of the outer vortices was strong. Then, if the strength of the inner vortices is weakened by the phase difference, the reattachment length is minimized, and if the strength of the inner vortices is strong, the mixing is enhanced.

INTRODUCTION

Coaxial jets in which a central jet is surrounded by an annular jet are commonly utilized where mixing between two jet streams is desired and often encountered in engineering applications such as gas turbine combustors, jet pumps, and chemical reactors, etc. Two turbulent shear layers exist in the coaxial jet flows which involve interaction and mixing, and near-field structures of the jet are considerably complex. The mixing between two streams is critically controlled by the dynamics and interactions of the vortical structures in shear layers developed between two jets and also between the annular jet and the ambient flow. Vortical structures can be altered by inflow conditions, i.e. velocity ratio of two jets (Dahm et al, 1992; Rehab et al. 1997), inflow pulsation frequency (Wicker and Eaton, 1994), etc. Understanding the dynamics of coaxial jets and finding a suitable pulsation condition are helpful to improve the mixing efficiency in combustion devices and industrial chemical systems.

Recently, several studies have concentrated on the manipulation of the vortical structures through active control. The mixing control by synthetic jets was studied by Ritchie et al. (2000). Angele et al. (2006) experimentally investigated the evolution of a three-dimensional structure and the mixing enhancement using the micro flap actuators. Balarac et al. (2007) and Mitsuishi et al. (2007) studied the effect of excitation using direct numerical simulations. The forcing was applied only on the outer shear layer because of its domination of the jet dynamics and they found that the mixing rate of coaxial jet flows can be critically altered by applying a suitable excitation.

In the present study, the effects of inflow pulsation on the flow characteristics and the mixing properties of a turbulent confined coaxial jet flows were studied. Large eddy simulations were carried out at Re = 9000, based on the bulk velocity and outer radius of annular jet. The mean velocity ratio of central to annular jets is 0.6. Main control parameters are the pulsation frequency ($0.1 < St < 0.9$) and the phase difference (ϕ) between annular and central jets. The pulsations at the annular and central jets were generated by varying the flow rate with 5% and 20%, respectively. The pulsation frequency responses were scrutinized by examining the phase- or time-averaged turbulent statistics. The pulsation frequencies of $St = 0.180$ and 0.327 gave the greatest enhancement in mixing and reduction of the reattachment length, respectively. Then, the effects of the phase difference between two inflow jets at the two optimal frequencies were investigated.

NUMERICAL METHOD

Many finite difference schemes have been constructed in physical space using cylindrical coordinates. However,

the mapping of independent variables is a useful tool for constructing finite difference methods on a non-uniform mesh (Morinish et al., 2004). In the present study, (x, r, θ) coordinates in physical space are mapped into (ζ^x, ζ^r, ζ^θ) in computational space, respectively.

A dynamic subgrid-scale stress model was used to account for subgrid-scale stresses (Germano et al., 1991; Lilly, 1992). Following the dynamic subgrid-scale model for scalar transport, the subgrid-scale mixture fraction transport was modeled assuming it was aligned with the scalar gradient vector (Moin et al., 1991).

The filtered and transformed governing equations for the continuity, incompressible Navier-Stokes and mixture fraction transport equations are

$$\frac{1}{J}\frac{\partial}{\partial\zeta^j}\left[\frac{J}{h_j}u_j\right]=0 \tag{1}$$

$$\frac{\partial u_x}{\partial t}+\frac{1}{J}\frac{\partial}{\partial\zeta^j}\left[\frac{J}{h_j}u_j u_x\right]=-\frac{1}{h_x}\frac{\partial p}{\partial\zeta^x}+\frac{1}{h_j}\frac{\partial\tau_{jx}}{\partial\zeta^j}+\frac{\tau_{rx}}{r} \tag{2}$$

$$\begin{aligned}&\frac{\partial u_r}{\partial t}+\frac{1}{J}\frac{\partial}{\partial\zeta^j}\left[\frac{J}{h_j}u_j u_r\right]-\frac{u_\theta u_\theta}{r}\\&=-\frac{1}{h_r}\frac{\partial p}{\partial\zeta^r}+\frac{1}{h_j}\frac{\partial\tau_{jr}}{\partial\zeta^j}+\frac{(\tau_{rr}-\tau_{\theta\theta})}{r}\end{aligned} \tag{3}$$

$$\begin{aligned}&\frac{\partial u_\theta}{\partial t}+\frac{1}{J}\frac{\partial}{\partial\zeta^j}\left[\frac{J}{h_j}u_j u_\theta\right]+\frac{u_r u_\theta}{r}\\&=-\frac{1}{h_\theta}\frac{\partial p}{\partial\zeta^\theta}+\frac{1}{h_j}\frac{\partial\tau_{j\theta}}{\partial\zeta^j}+2\frac{\tau_{r\theta}}{r}\end{aligned} \tag{4}$$

$$\frac{\partial f}{\partial t}+\frac{1}{J}\frac{\partial}{\partial\zeta^j}\left[\frac{J}{h_j}u_j f\right]=\frac{1}{h_j}\frac{\partial q_j}{\partial\zeta^j}+\frac{q_j}{r} \tag{5}$$

where τ_{ij} are the viscous shear stresses and q_j are the scalar fluxes.

All variables are non-dimensionalized by the bulk velocity (U_o) and outer radius (R_o) of annular jet. The Reynolds number based on the bulk velocity and outer radius of annular jet is 9000. The working fluid is air; hence the Schmidt number (Sc) is 1.

The governing equations are integrated in time using the fractional step method with the implicit velocity decoupling procedure proposed by Kim et al. (2002). Under this approach, the terms are first discretized in time using the Crank-Nicholson method, and then the coupled velocity components in the convection terms are decoupled using the implicit velocity decoupling procedure. The decoupled velocity components are then solved without iteration. Since the implicit decoupling procedure relieves the Courant-Friedrichs-Lewy restriction, the computation time is reduced significantly. The overall accuracy in time is second-order. All the terms are resolved using a second-order central difference scheme in space with a staggered mesh, while the convection terms in Eq. (5) are resolved using the bounded QUICK scheme to avoid significant numerical instability (Akselvoll and Moin, 1995; Herrmann and Blanquart, 2006). Details regarding the numerical algorithm can be found in the paper of Kim et al. (2002). Using the homogeneity in the azimuthal direction, the three-dimensional Poisson equation is reduced to a set of decoupled two-dimensional Helmholtz equations through Fourier decomposition. Each Fourier mode is solved with a multigrid algorithm to accelerate the convergence of the iterative procedure.

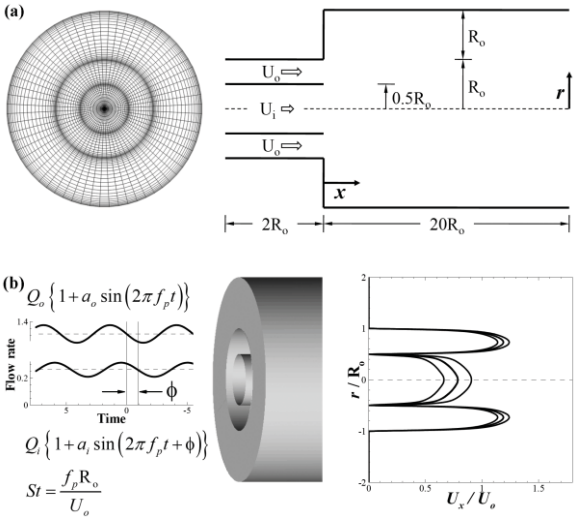

Figure 1: (a) Schematic of computational domain, (b) inflow pulsation.

A schematic of the computational domain and inflow pulsation are shown in Figure 1(a). The numbers of grid points in the x, r and θ directions were 305×105×129, respectively. 80 of the 305 axial grid points were used to cover the inlet section (upstream of the expansion). In the axial and radial directions, grid points were clustered along all solid walls. The time step was 0.0058 R_o/U_o and the total averaging time was 611 R_o/U_o. At each time step, stored two-dimensional instantaneous velocity data obtained from a simulation of periodic turbulent pipe and annular flow with pulsation were provided at the inlet of the main simulation. Pulsations are superimposed on the inflows of annular and central jets. The mean velocity ratio of central to annular jets, U_i / U_o, is 0.6. The pulsation at the inflow jets was generated by varying the flow rate according to the equation:

$$Q_{annular}=Q_o\left\{1+a_o\sin(2\pi f_p t)\right\} \tag{6}$$

$$Q_{central}=Q_i\left\{1+a_i\sin(2\pi f_p t+\phi)\right\} \tag{7}$$

where ϕ is the phase difference between annular and central jets and f_p is the pulsation frequency. The pulsation amplitudes of annular and central jets were 5% (a_o) and 20% (a_i), respectively. The pulsation frequency was given in a range $0.1 < St < 0.9$ where the definition of St is $St = f_p R_o/U_o$ while other parameters were fixed. The convective boundary condition $\partial u/\partial t + U_c\partial u/\partial x = 0$ was used at the exit, where U_c is taken to be the mean exit velocity.

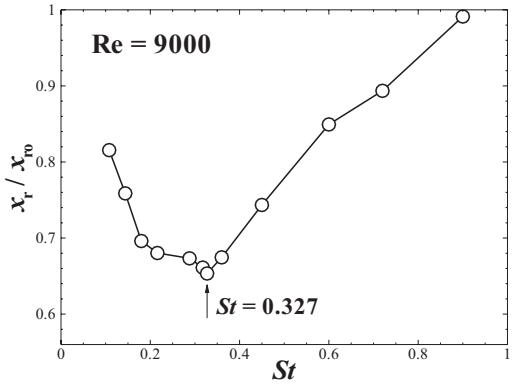

Figure 2: Pulsation frequency effect on the mean reattachment length.

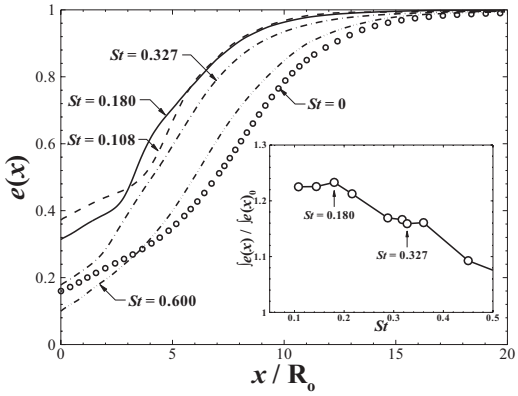

Figure 3: Pulsation frequency effect on the mixing efficiency.

Periodic boundary conditions were applied in the azimuthal direction for the velocity components, and no-slip boundary conditions were imposed at the solid walls. For the mixture fraction, periodic boundary condition was used in the azimuthal direction. The Neumann condition was applied along all solid walls. The inflow boundary condition was determined using a Dirichlet condition: $f = 1$ at the central jet, and $f = 0$ at the annular jet. The convective boundary condition was the same as that of momentum equations.

EFFECTS OF THE PULSATION FREQUENCY

First, we examine the effect of inflow pulsation frequency on the mean reattachment length. Figure 2 shows the variation of the mean reattachment length for pulsation frequency. The pulsation frequency is given in a range $0.1 < St < 0.9$ while other parameters are fixed. The reattachment length is normalized by that of no-pulsation, $x_{r0}/R_o = 9.907$ at $St = 0$. We found that the reattachment length is most reduced at $St = 0.327$ by the amount of 34.7% than that of no-pulsation. When St is less (more) than 0.327, the reattachment length increases as St decreases (increases). The reduction of reattachment length is more than 30% in a range $0.180 < St < 0.360$, this range is the same from quarter- to half-harmonic St predicted by the linear stability theory, $St_o = f_p\theta_o/U$=0.033 (St = 0.721).

Figure 3 shows the variation of the mixing efficiency due to pulsation frequency along the streamwise distance. The mixing efficiency is defined as,

$$e(x) = 1 - \frac{\int |f(x,r) - f_\infty| \, dA}{\int |f_0(x,r) - f_\infty| \, dA} \tag{8}$$

where $f_o(x,r)$ is 1 for $0 < r/R_o < 1/2$ and 0 for otherwise, and f_∞ is the mixture fraction associated with a completely mixed state, $f_\infty = 0.1667$. The mixing efficiency monotonically increases from the expansion point along the streamwise distance and approaches gradually 1, completely mixed state, at the end of simulation domain for all cases. Near the expansion point ($x/R_o < 3$), the mixing efficiency increases as St decreases. For low St cases (0.108, 0.180), the mixing efficiency undergoes a brutal growth in a range $3 < x/R_o < 6$. To investigate the overall effect of pulsation frequency on mixing enhancement, we defined the global mixing efficiency as the integral of the mixing efficiency along the streamwise distance from the expansion point to the end of domain. The global mixing efficiency is normalized by that of no-pulsation. The global mixing efficiency of all inflow pulsation cases is higher than that of no-pulsation case. In Figure 3, the mixing is most enhanced at $St = 0.180$. When St is more than 0.180, the global mixing efficiency decreases as St increases. The optimal pulsation frequency, $St = 0.180$, for the mixing enhancement is the same as the frequency of the general wake instability like as the vortex shedding frequency behind a sphere.

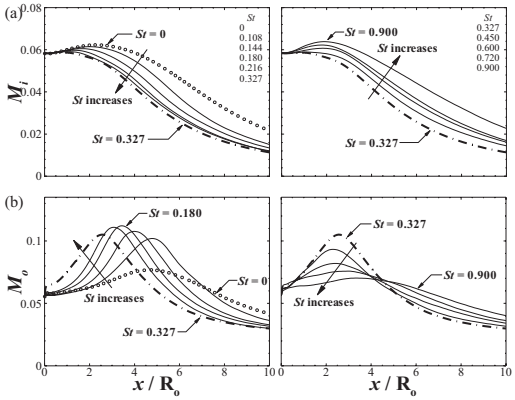

Figure 4: Momentum flux. (a) inner, (b) outer shear layer.

Figure 4 shows the variation of the momentum flux along the streamwise distance. We define the following quantities M_i for the inner shear layer and M_o for the outer shear layer by

$$M_i(x) = \frac{1}{A}\int\int_0^{\frac{3}{4}R_o} (u_x^2 + u_r^2 + u_\theta^2) r dr d\theta$$
$$M_o(x) = \frac{1}{A}\int\int_{\frac{3}{4}R_o}^{2R_o} (u_x^2 + u_r^2 + u_\theta^2) r dr d\theta \tag{9}$$

where A is the cross-sectional area of the chamber. The momentum flux in the inner shear layer is smallest at St = 0.327, where the reattachment length is smallest, due to the better homogeneity of axial velocity component. The momentum flux in the outer shear layer is largest at St = 0.180, where the mixing is most enhanced. The x-location for the maximum M_o shifts downstream as St decreases for St < 0.45. The global trends of M_i are similar to the variation of the reattachment length as shown in Figure 2, and the variation of the maximum values of M_o is similar to the mixing enhancement. Thus, when the pulsation frequency is only the control parameter, M_i and M_o seem to represent the variation of the reattachment length and the mixing enhancement, respectively.

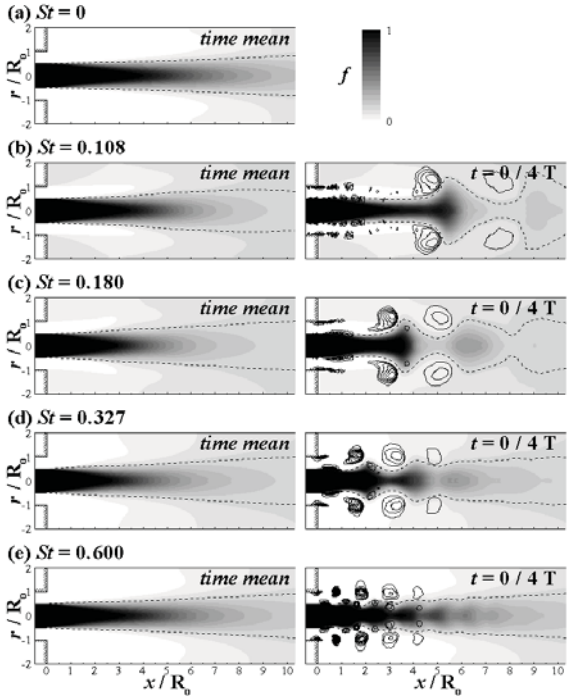

Figure 5: Averaged mixture fraction and spanwise vortical structures (λ_{ci}). The contour levels of λ_{ci} are from 0.25 to 5 by increments of 0.25.
Left: time-averaged, Right: phase-averaged.
Dashed line: f = 0.1667

Left and right figures of Figure 5 show the time- and phase-averaged mixture fraction, respectively. The snapshots of the phase-averaged mixture fraction were taken at t = 0/4 T where T is the pulsation period. It is seen that the stream issued from the central jet more exists near the corner of expansion point as St decreases. The mixing efficiency is then higher as St decreases near the expansion point as shown in Figure 3. The vortex identification method of Zhou et al. (1999) was adopted to visualize the vortical structures by using a contour of swirling strength λ_{ci}. In right figures of Figure 5, two-dimensional swirling strength λ_{ci} (indicated by solid lines) clearly shows the azimuthal vortical structures due to the inflow pulsation, and those vortices convect downstream over time. The rotation direction of the azimuthal vortices is indicated in Figure 8(c). The inner vortex rotates in the opposite direction to the outer vortex. The inner vortex is trapped in the free space between two consecutive outer vortices in Figure 8(b, c, d). This is the locking phenomenon reported by many previous studies. At St = 0.600, the inner vortex is divided into two parts due to the strong outer vortex. One is trapped between outer vortices like other cases, and the other is located beneath outer vortex as shown in Figure 8(e). The first outer spanwise vortex is formed faster and the distance between two outer vortices is closer as St increases. The x-location for the first outer spanwise vortex at t = 0/4 T and the distance between two outer vortices is closer as St increases. However, the radius of outer vortical structure is larger as St decreases. Dashed line is the mixture fraction of the completely mixed state, f_∞ = 0.1667. It is seen that the outer vortices pinch inner shear layer indicated by dashed line. This pinching effect makes that central jet expands in the radial direction at the front of outer vortex, and annular jet invades at the back of outer vortex. Thus, the mushroom-shaped structures are shown by the blue line. When the mushroom-shaped structures are generated, the mixture fraction in the center region of the structures diffuses quickly in the radial direction. The interface area between two inflow jets increases because the stream issued from the central jet invades the annular jet region and the annular jet penetrates the center line. This structure enhances large scale mixing due to coherent structure. However, at St = 0.108, the distance in the radial direction between two blue lines decreases after about x/R_o = 9 due to this structure.

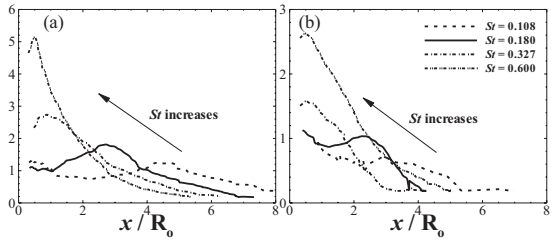

Figure 6: Swirling strength of vortex center. (a) outer shear layer, (b) inner shear layer.

Figure 6 shows the variation of the swirling strength of vortex center due to inflow pulsation. The x-location of the maximum swirling strength of outer vortex shifts downstream with decreasing St. The maximum value and the increasing rate of the swirling strength of outer vortex increase with increasing St. The swirling strength of outer vortex is twice as large as that of inner vortex.

EFFECTS OF THE PHASE DIFFERENCE BETWEEN TWO INFLOW JETS

To investigate the effect of the phase difference between two inflow jets, we performed large eddy simulations using the same pulsation inflow with 30° increments of the phase difference for two optimal pulsation frequencies; one is St = 0.327 for the minimum reattachment length and the other is St = 0.180 for the mixing enhancement.

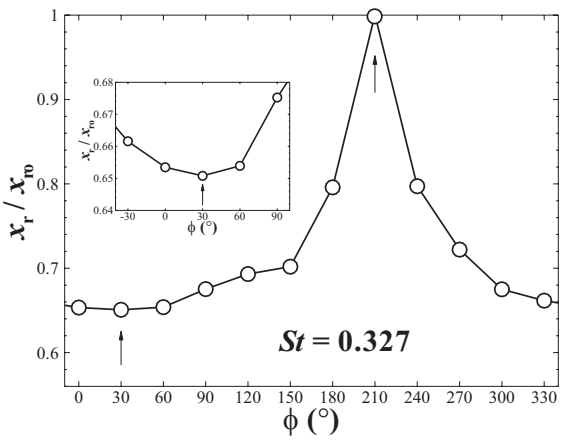

Figure 7: Phase difference effect on the mean reattachment length with $St = 0.327$.

Figure 7 shows the variation of the reattachment length for the phase difference at $St = 0.327$. We found that the reattachment length is most reduced at $\phi = 30°$ by the amount of 34.9%. $\phi = 30°$ reduces the reattachment length more by the amount of $0.026R_o$ (0.4%) than $\phi = 0°$. It is seen that the reattachment length significantly increases in a range $150° < \phi < 240°$. For $\phi = 210°$, the reattachment length is almost the same as that of no-pulsation. The variation seems to be symmetric about $\phi = 30°$ (or 210°).

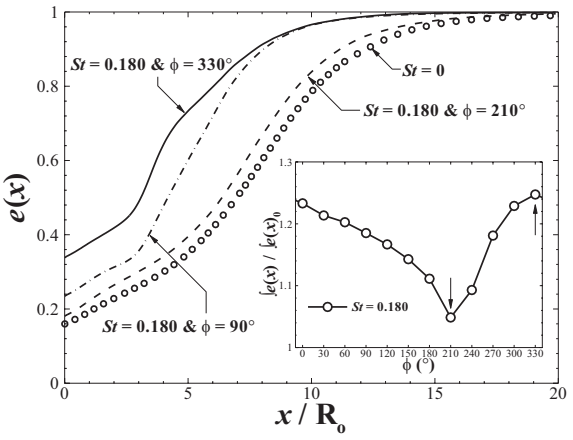

Figure 8: Phase difference effect on the mixing efficiency with $St = 0.180$.

Figure 8 shows the variation of the mixing efficiency for the phase difference at $St = 0.180$. The most effective phase difference for mixing enhancement is obtained at $\phi = 330°$. $\phi = 330°$ increases the mixing efficiency more by the amount of 0.26% than $\phi = 0°$ in a range $0 < x/R_o < 8$. For $\phi = 210°$, the trend of the mixing efficiency is similar to that of no-pulsation. However, the mixing efficiency is higher than no-pulsation by the amount of 5%. The global mixing efficiency gradually decreases as ϕ increases from 330° (-30°) to 210°, and abruptly increases as ϕ increases from 210° to 330°.

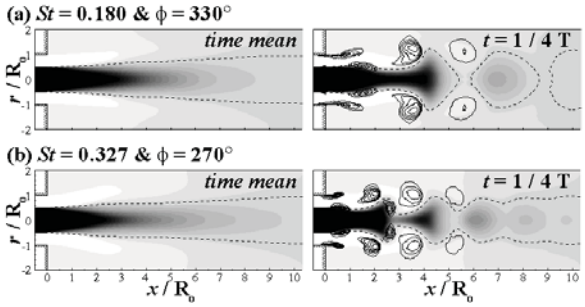

Figure 9: Averaged mixture fraction and spanwise vortical structures. (a) $St = 0.180$, (b) $St = 0.327$

Figure 9(a) and 9(b) show the time- and phase-averaged mixture fraction at optimal phase difference for mixing enhancement at $St = 0.180$ and 0.327, respectively. The global mixing efficiencies are 1.25 for $St = 0.180$ with $\phi = 330°$ and 1.20 for $St = 0.327$ with $\phi = 270°$. For $St = 0.180$ with $\phi = 330°$, which is most mixing enhanced case among the all cases, the mushroom-shaped structure is detached from the main central jet stream, about $x/R_o = 5$. When the structure is detached, the outer jet penetrates to the center line. For $St = 0.327$ with $\phi = 270°$, the stream issued from the central jet exists near the corner of expansion point in contrast with Figure 8(c). And the mushroom-shaped structure is also observed.

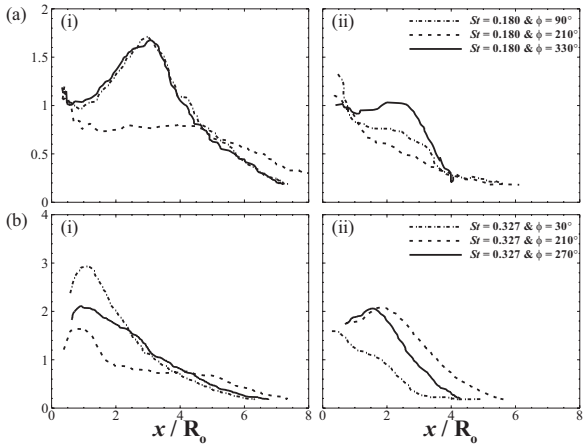

Figure 10: Swirling strength of vortex center. (a) $St = 0.180$, (b) $St = 0.327$. (i) outer shear layer, (ii) inner shear layer

Figure 10 shows the variation of the swirling strength of vortex center due to phase difference. When the reattachment length is minimized (indicated by dash dot line; $St = 0.180$ & $\phi = 90°$, $St = 0.327$ & $\phi = 30°$), it is seen that the outer swirling strength is large but the inner swirling strength is small. When the mixing is enhanced (indicated by solid line; $St = 0.180$ & $\phi = 330°$, $St = 0.327$ & $\phi = 270°$), it is seen that the both outer and inner swirling strength are somewhat large. In this case, the positive and negative large u_r, which is located at the front and back of the outer vortex, is expanded near the center line by the strong inner vortex. So the central jet is expanded to the later wall of the chamber, and the annular jet penetrates to

the center line. Thus, the mushroom-shaped structures are made. For ϕ = 210° both St = 0.180 and 0.327, the outer swirling strength is the weakest and the effects of the inflow pulsation are the weakest. However, the inner swirling strength for St = 0.327 with ϕ = 210° is large. Thus, the outer vortex is dominant for the effects of the phase difference.

CONCLUSIONS

Large eddy simulations of incompressible turbulent flow through a coaxial jet were performed at Re = 9000 to investigate the effects of inflow pulsation. The mean velocity ratio of central to annular jets was 0.6. The pulsation at the inflow jets was generated by varying the flow rate. The pulsation amplitudes of annular and central jets were 5% and 20%, respectively.

To investigate the effects of the pulsation frequency, the pulsation frequency was given in a range $0.1 < St < 0.9$ while other parameters are fixed. The reduction of the reattachment length was more than 30% from quarter- (St = 0.180) to half-harmonic (St = 0.360) frequency predicted by the linear stability theory. The maximum reduction of the reattachment length, 34.7%, was obtained at St = 0.327. At this frequency, the momentum flux in the inner shear layer was smallest and all turbulent intensities inside the recirculation zone were maximized in a range $x/R_o < 3$. The mixing was most enhanced at St = 0.180, which is the same as the frequency of the general wake instability. At this frequency, the momentum flux in the outer shear layer was largest and the pinching effect, which made the mushroom-shaped structures and enhanced the large scale mixing, was intensified.

To investigate the effect of the phase difference between two inflow jets, we performed large eddy simulations using the same pulsation inflow with 30° increments of the phase difference for two optimal pulsation frequencies; one is St = 0.327 for the minimum reattachment length and the other is St = 0.180 for the mixing enhancement. We found that the reattachment length is most reduced at St = 0.327 with ϕ = 30° by the amount of 34.9%. When the reattachment length is minimized, it is seen that the outer swirling strength is large but the inner swirling strength is small. The most effective phase difference for mixing enhancement was obtained at St = 0.180 with ϕ = 330°. In this case, the positive and negative large u_r, which is located at the front and back of the outer vortex, was expanded near the center line by the strong inner and outer vortices. The mushroom-shaped structures were made. From the r.m.s of the mixture fraction, both the turbulent and the large scale mixing are dominant for the mixing enhanced cases. The optimal conditions of the phase difference in the mixing enhancement and the reduction of the reattachment length were obtained when the strength of the outer vortices was strong. Then, if the strength of the inner vortices weakened by the phase difference, the reattachment length is minimized, and if the strength of the inner vortices was strong, the mixing is enhanced.

ACKNOWLEDGEMENT

The authors acknowledge the support of the KISTI under Grand Challenge Supercomputing Program (KSC-2008-G2-0001).

REFERENCES

Akselvoll, K., and Moin, P., 1995, Report No. TF-63, Thermosciences Division, Department of Mechanical Engineering, Stanford University.

Angele, K., Kurimoto, N., Suzuki, Y., and Kasagi, N., 2006, "Evolution of the streamwise vortices in coaxial jet controlled with micro flap actuators", *J. Turbulence*, Vol. 7, 73.

Balarac, G., Metais, O., and Lesieur, M., 2007, "Mixing enhancement in coaxial jets through inflow forcing: A numerical study", *Phys. Fluids*, Vol. 19, 075102.

Germano, M., Piomelli, U., Moin, P., and Cabot, W.H., 1991, "A dynamic subgrid-scale eddy viscosity model", *Phys. Fluids*, Vol. 3, pp. 1760–1765.

Herrmann, M., and Blanquart, G. 2006, "Flux corrected finite volume scheme for preserving scalar boundedness in reacting large-eddy simulations", *AIAA*, Vol. 44, pp. 2879-2886.

Kim, K., Baek, S. J., and Sung, H. J., 2002, "An implicit velocity decoupling procedure for the incompressible Navier-Stokes equations" *Int. J. Numer. Meth. Fluids*, Vol. 38, pp. 125-138.

Lilly, D.K., 1992, "A proposed modification of the Germano subgridscale closure method", *Phys. Fluids*, Vol. 4, pp. 633–635.

Misuishi, A., Fukagata, K., and Kasgi, N., 2007, "Near-field development of large-scale vortical structures in a controlled confined coaxial jet", *J. Turbulence*, Vol. 8, 23.

Moin, P., Squires, K., Cabot,W., and Lee, S., 1991, "A dynamic subgrid-scale model for compressible turbulence and scalar transport", *Phys. Fluids*, Vol. 3, pp. 2746–2757.

Morinishi, Y., Vasilyev, O.V., and Ogi, T., 2004, "Fully conservative finite difference scheme in cylindrical coordinates for incompressible flow simulations", *J. Comput. Phys.*, Vol. 197, pp. 686–710.

Rehab, H., Villermaux, E., and Hopfinger, E. J., 1997, "Flow regimes of large-velocity-ratio coaxial jets", *J. Fluid Mech*. Vol. 345, pp. 357-381

Ritchie, B.D., Mujumdar, D.R., and Seitzman, J.M., 2000, "Mixing in coaxial jets using synthetic jet actuators", *AIAA*.

Wicker R. B., and Eaton, J. K., 1994, "Near field of a coaxial jet with and without axial excitation", *AIAA*, Vol. 32, pp. 542-546.

Zhou, J., Adrian, R. J., Balachandar, S., and Kendall, T. M., 1999, "Mechanisms for generating coherent packets of hairpin vortices in channel flow", *J. Fluid Mech*. Vol. 387, pp. 353-396.